Stanford Exploration Project, Report 124, April 4, 2006, pages 31–45

Generalized Riemannian wavefield extrapolation

Jeff Shragge

ABSTRACT

This paper extends wavefield extrapolation to generalized Riemannian spaces. The key component is the development of a dispersion relationship appropriate for propagating wavefield on generalized non-orthogonal meshes. This wavenumber contains a number of mixed-domain fields in addition to velocity that represent coordinate system geometry. An extended split-step Fourier approximation of the extrapolation wavenumber is developed, which provides accurate results when multiple reference parameters sets are used. Three examples are presented that demonstrate the validity of the theory. An important consequence is that greater emphasis can be placed on generating smoother computational meshes rather than satisfying restrictive semi-orthogonal criteria. This result should lead to more accurate and efficient generalized Riemannian wavefield extrapolation.

INTRODUCTION

Riemannian wavefield extrapolation (RWE) (Sava and Fomel, 2005) generalizes wavefield extrapolation to non-Cartesian coordinate systems. The original formulation assumed that coordinate systems are at least semi-orthogonal and characterized by an extrapolation direction orthogonal to the other two axes. This supposition resulted in a wave-equation dispersion relationship for the extrapolation wavenumber containing mixed-domain fields additional to velocity that encode coordinate system geometry. However, semi-orthogonal geometry can be an overly restrictive assertion because many computational meshes have greatly varying mixed-domain coefficients that cause numerical instability during wavefield extrapolation.

Initially, RWE was designed for dynamic applications where wavefields are extrapolated on ray-based coordinate systems oriented in the wave propagation direction. This approach generally generates high-quality Green's functions; however, numerical instability (i.e. zero divisions) occurs wherever the ray coordinate system triplicates. Sava and Fomel (2005) addressed this issue by iteratively smoothing the velocity model until coordinate system triplications vanish. This solution, though, is somewhat less than ideal because it counters the original purpose of RWE: coordinate systems conformal to propagation directions.

A second more geometric RWE application is performing wavefield extrapolation to and from surfaces of irregular geometry. Shragge and Sava (2004) formulate a wave-equation migration from topography strategy that poses wavefield extrapolation directly in locally orthogonal meshes conformal to the acquisition surface. Although successful in areas with longer wavelength and lower amplitude topography, imaging results degraded in situations involv-

ing more rugged acquisition topography. However, a more general observation is the genetic link between degraded image quality and the grid compression/extension demanded by semi-orthogonality.

A solution to these two problems is to extend RWE to include non-orthogonal coordinate systems. This generalized RWE (GRWE) framework removes the semi-orthogonal constraint to allow propagation in non-orthogonal Riemannian spaces. Non-orthogonality introduces two additional terms in the GRWE dispersion relationship and makes existing coefficient terms slightly more involved. The non-stationary coefficients in the resulting extrapolation wavenumber can be handled with an extended split-step Fourier approach (Stoffa et al., 1990). Importantly, this solution affords greater flexibility in coordinate system design while facilitating more rapid mesh generation. Furthermore, greater emphasis can be placed on optimizing grid quality by controlling grid clustering and generating smoother coefficient fields (Shragge, 2006b).

This paper develops the 3D wave-equation dispersion relationship for performing GRWE. I first discuss generalized Riemannian geometry and show how the acoustic wave-equation can be formulated in a non-orthogonal Riemannian space. Subsequently, I develop an expression for a one-way wavefield extrapolation wavenumber and present the corresponding split-step Fourier approximation. I then present two analytic 2-D non-orthogonal coordinate systems to help validate the developed extrapolation wavenumber expressions. The paper concludes with a more realistic example of GRWE generated Green's function estimates through a slice of the SEG-EAGE salt model.

GENERALIZED RIEMANNIAN GEOMETRY

Geometry in a generalized 3D Riemannian space is described by a symmetric metric tensor, $g_{ij} = g_{ji}$, that relates the geometry in a non-orthogonal coordinate system, $\{x_1, x_2, x_3\}$, to an underlying Cartesian mesh, $\{\xi_1, \xi_2, \xi_3\}$ (Guggenheimer, 1977). In matrix form, the metric tensor is written,

$$\left[g_{ij}\right] = \begin{bmatrix} g_{11} & g_{12} & g_{13} \\ g_{21} & g_{22} & g_{23} \\ g_{31} & g_{32} & g_{33} \end{bmatrix} = \begin{bmatrix} g_{11} & g_{12} & g_{13} \\ g_{12} & g_{22} & g_{23} \\ g_{13} & g_{23} & g_{33} \end{bmatrix}, \tag{1}$$

where g_{11}, g_{12}, g_{22}, g_{13}, g_{23} and g_{33} are functions linking the two coordinate systems through,

$$\begin{aligned} g_{11} &= \frac{\partial x_k}{\partial \xi_1}\frac{\partial x_k}{\partial \xi_1}, \quad g_{12} = \frac{\partial x_k}{\partial \xi_1}\frac{\partial x_k}{\partial \xi_2}, \quad g_{22} = \frac{\partial x_k}{\partial \xi_2}\frac{\partial x_k}{\partial \xi_2}, \\ g_{13} &= \frac{\partial x_k}{\partial \xi_1}\frac{\partial x_k}{\partial \xi_3}, \quad g_{23} = \frac{\partial x_k}{\partial \xi_2}\frac{\partial x_k}{\partial \xi_3}, \quad g_{33} = \frac{\partial x_k}{\partial \xi_3}\frac{\partial x_k}{\partial \xi_3}. \end{aligned} \tag{2}$$

(Summation notation - $g_{ii} = g_{11} + g_{22} + g_{33}$ - is used in equations throughout this paper.) The associated (or inverse) metric tensor, g^{ij}, is defined by $g_{ij} = |\mathbf{g}|\, g^{ij}$, where $|\mathbf{g}|$ is metric tensor

matrix determinant. The associated metric tensor is given by,

$$\left[g^{ij}\right] = \frac{1}{|\mathbf{g}|}\begin{bmatrix} g_{22}g_{33}-g_{23}^2 & g_{13}g_{23}-g_{12}g_{33} & g_{12}g_{23}-g_{13}g_{22} \\ g_{13}g_{23}-g_{12}g_{33} & g_{11}g_{33}-g_{13}^2 & g_{12}g_{13}-g_{11}g_{23} \\ g_{12}g_{23}-g_{13}g_{22} & g_{12}g_{13}-g_{11}g_{23} & g_{11}g_{22}-g_{12}^2 \end{bmatrix}, \tag{3}$$

and has the following metric determinant,

$$|\mathbf{g}| = g_{33}\left(g_{11}g_{22}-g_{12}^2\right)\left[1-\frac{g_{11}g_{23}^2+g_{22}g_{13}^2-2g_{12}g_{23}g_{13}}{g_{33}(g_{11}g_{22}-g_{12}^2)}\right]. \tag{4}$$

Weighted metric tensor, $m^{ij} = \sqrt{|\mathbf{g}|}\, g^{ij}$, is a useful definition for the following development.

ACOUSTIC WAVE-EQUATION IN 3D GENERALIZED RIEMANNIAN SPACES

The acoustic wave-equation for wavefield, $\mathcal{U}$, in a generalized Riemannian space is,

$$\Delta\mathcal{U} = -\omega^2 s^2(\mathbf{x})\,\mathcal{U}, \tag{5}$$

where the ω is frequency, s is the propagation slowness, and Δ is the Laplacian operator,

$$\Delta\mathcal{U} = \frac{1}{\sqrt{|\mathbf{g}|}}\frac{\partial}{\partial\xi_i}\left(m^{ij}\frac{\partial\mathcal{U}}{\partial\xi_j}\right). \tag{6}$$

Substituting equation 6 into 5 generates a Helmholtz equation appropriate for propagating waves through a 3D space,

$$\frac{1}{\sqrt{|\mathbf{g}|}}\frac{\partial}{\partial\xi_i}\left(m^{ij}\frac{\partial\mathcal{U}}{\partial\xi_j}\right) = -\omega^2 s^2\mathcal{U}. \tag{7}$$

Expanding the derivative terms and multiplying through by $\sqrt{|\mathbf{g}|}$ yields ,

$$\frac{\partial m^{ij}}{\partial\xi_i}\frac{\partial\mathcal{U}}{\partial\xi_j} + m^{ij}\frac{\partial^2\mathcal{U}}{\partial\xi_i\partial\xi_j} = -\sqrt{|\mathbf{g}|}\omega^2 s^2\mathcal{U}. \tag{8}$$

Defining n_j as,

$$n_j = \frac{\partial m^{ij}}{\partial\xi_i} = \frac{\partial m^{1j}}{\partial\xi_1} + \frac{\partial m^{2j}}{\partial\xi_2} + \frac{\partial m^{3j}}{\partial\xi_3}, \tag{9}$$

leads to a more compact notation of equation 8,

$$n_j\frac{\partial\mathcal{U}}{\partial\xi_j} + m^{ij}\frac{\partial^2\mathcal{U}}{\partial\xi_i\partial\xi_j} = -\sqrt{|\mathbf{g}|}\omega^2 s^2\mathcal{U}. \tag{10}$$

Developing a wave-equation dispersion relation is achieved by replacing the partial differential operators acting on wavefield $\mathcal{U}$ with their Fourier domain duals,

$$\left(m^{ij}k_{\xi_i} - in_j\right)k_{\xi_j} = \sqrt{|\mathbf{g}|}\omega^2 s^2, \tag{11}$$

where k_{ξ_i} is the Fourier domain dual of differential operator $\frac{\partial}{\partial\xi_i}$. Equation 11 represents the dispersion relationship for wavefield propagation on a generalized 3-D Riemannian space.

One-way wavefield extrapolation

Developing an expression for the extrapolation wavenumber requires isolating one of the wavenumbers in equation 11 (herein assumed to be coordinate ξ_3). Rearranging the results of expanding equation 11 by introducing indicies $i, j = 1,2,3$ yields,

$$\begin{aligned} m^{33}k_{\xi_3}^2 + \left(2m^{13}k_{\xi_1} + 2m^{23}k_{\xi_2} - i\,n_3\right)k_{\xi_3} = \\ \sqrt{|\mathbf{g}|}\omega^2 s^2 + i\left(n_1 k_{\xi_1} + n_2 k_{\xi_2}\right) - m^{11}k_{\xi_1}^2 - m^{22}k_{\xi_2}^2 - 2m^{12}k_{\xi_1}k_{\xi_2}. \end{aligned} \tag{12}$$

An expression for wavenumber k_{ξ_3} can be obtained by completing the square,

$$\begin{aligned} m^{33}\left(k_{\xi_3} + \tfrac{\left(2m^{13}k_{\xi_1} + 2m^{23}k_{\xi_2} - i\,n_3\right)}{2m^{33}}\right)^2 = \sqrt{|\mathbf{g}|}\omega^2 s^2 - k_{\xi_1}^2\left(m^{11} - \tfrac{\left(m^{13}\right)^2}{m^{33}}\right) - \\ k_{\xi_2}^2\left(m^{22} - \tfrac{\left(m^{23}\right)^2}{m^{33}}\right) - k_{\xi_1}k_{\xi_2}\left(2m^{12} - \tfrac{2m^{13}m^{23}}{m^{33}}\right) + i\,k_{\xi_1}\left(n_1 - \tfrac{m^{13}n_3}{m^{33}}\right) + i\,k_{\xi_2}\left(n_2 - \tfrac{m^{23}n_3}{m^{33}}\right) - \tfrac{n_3^2}{m^{33}}. \end{aligned} \tag{13}$$

Isolating wavenumber k_{ξ_3} yields,

$$k_{\xi_3} = -a_1 k_{\xi_1} - a_2 k_{\xi_2} + i a_3 \pm \left[a_4^2\omega^2 - a_5^2 k_{\xi_1}^2 - a_6^2 k_{\xi_2}^2 - a_7 k_{\xi_1}k_{\xi_2} + a_8 i\,k_{\xi_1} + a_9 i\,k_{\xi_2} - a_{10}^2\right]^{\frac{1}{2}}, \tag{14}$$

where a_i are non-stationary coefficients given by,

$$\mathbf{a} = \left[\frac{g^{13}}{g^{33}} \quad \frac{g^{23}}{g^{33}} \quad \frac{n_3}{2m^{33}} \quad \frac{s}{\sqrt{g^{33}}} \quad \sqrt{\frac{g^{11}}{g^{33}} - \left(\frac{g^{13}}{g^{33}}\right)^2} \quad \sqrt{\frac{g^{22}}{g^{33}} - \left(\frac{g^{23}}{g^{33}}\right)^2} \quad \left[\frac{2g^{12}}{g^{33}} - \frac{2g^{13}g^{23}}{\left(g^{33}\right)^2}\right] \quad \left[\frac{n_1}{m^{33}} - \frac{m^{13}n_3}{\left(m^{33}\right)^2}\right] \quad \left[\frac{n_2}{m^{33}} - \frac{m^{23}n_3}{\left(m^{33}\right)^2}\right] \quad \frac{n_3}{m^{33}}\right]^{\mathbf{T}}. \tag{15}$$

Note that the coefficients contain a mixture of m^{ij} and g^{ij} terms, and that positive definite terms, a_4, a_5, a_6 and a_{10} in equation 14, are squared such that the familiar Cartesian split-step Fourier correction is recovered below.

Split-Step Fourier Approximation

The extrapolation wavenumber defined in equations 14 and 15 cannot be implemented purely in the Fourier domain due to the presence of mixed-domain fields (i.e. a function of both ξ_1 and k_{ξ_1} simultaneously). This can be addressed using an extended version of the split-step Fourier approximation (Stoffa et al., 1990), a popular approach that uses Taylor expansions to separate k_{ξ_3} into two parts: $k_{\xi_3} \approx k_{\xi_3}^{PS} + k_{\xi_3}^{SSF}$. Wavenumbers $k_{\xi_3}^{PS}$ and $k_{\xi_3}^{SSF}$ represent a pure Fourier domain phase-shift and a mixed $\omega - \mathbf{x}$ domain split-step correction, respectively.

The phase-shift term is given by,

$$k_{\xi_3}^{PS} = -b_1 k_{\xi_1} - b_2 k_{\xi_2} + i b_3 \pm \left[b_4^2\omega^2 - b_5^2 k_{\xi_1}^2 - b_6^2 k_{\xi_2}^2 - b_7 k_{\xi_1}k_{\xi_2} + b_8 i\,k_{\xi_1} + b_9 i\,k_{\xi_2} - b_{10}^2\right]^{\frac{1}{2}}, \tag{16}$$

where $b_i = b_i(\xi_3)$ are reference values of $a_i = a_i(\xi_1, \xi_2, \xi_3)$. The split-step approximation is developed by performing a Taylor expansion about each coefficient a_i and evaluating the

results at stationary reference values b_i. The stationary values of k_{ξ_1} and k_{ξ_2} are assumed to be zero. This leads to a split-step correction of,

$$k_{\xi_3}^{SSF} = \left.\frac{\partial k_{\xi_3}}{\partial a_3}\right|_0 (a_3 - b_3) + \left.\frac{\partial k_{\xi_3}}{\partial a_4}\right|_0 (a_4 - b_4) + \left.\frac{\partial k_{\xi_3}}{\partial a_{10}}\right|_0 (a_{10} - b_{10}), \tag{17}$$

where “0” denotes "with respect to a reference medium". The partial differential expressions in equation 17 are,

$$\left.\frac{\partial k_{\xi_3}}{\partial a_3}\right|_0 = b_3, \quad \left.\frac{\partial k_{\xi_3}}{\partial a_4}\right|_0 = \frac{b_4\,\omega^2}{\sqrt{b_4^2\,\omega^2 - b_{10}^2}}, \quad \left.\frac{\partial k_{\xi_3}}{\partial a_{10}}\right|_0 = -\frac{b_{10}}{\sqrt{b_{10}^2\,\omega^2 - b_{10}^2}}, \tag{18}$$

resulting in the following split-step Fourier correction,

$$k_{\xi_3}^{SSF} = i\,b_3\,(a_3 - b_3) + \frac{b_4\,\omega^2\,(a_4 - b_4)}{\sqrt{b_4^2\,\omega^2 - b_{10}^2}} - \frac{b_{10}\,(a_{10} - b_{10})}{\sqrt{b_4\,\omega^2 - b_{10}^2}}. \tag{19}$$

Note that we could use many reference media followed by interpolation similar to the phase-shift plus interpolation (PSPI) technique of Gazdag and Sguazzero (1984).

Importantly, even though there are additional a_i coefficients in the dispersion relationship, these can be made smooth through mesh regularization such that fewer sets of reference parameters are needed to accurately represent wavenumber k_{ξ_3}. In addition, situations exist where some coefficients are zero or negligible. For example, the coefficients for a weakly non-orthogonal coordinate system (i.e. $\max|\{g^{12}, g^{13}, g^{23}\}| << \max\{g^{11}, g^{22}, g^{33}\}$) within a kinematic approximation reduce to,

$$\mathbf{a} \approx \left[0 \;\; 0 \;\; 0 \;\; s/\sqrt{g^{33}} \;\; \sqrt{g^{11}/g^{33}} \;\; \sqrt{g^{22}/g^{33}} \;\; 0 \;\; 0 \;\; 0 \;\; n_3/m^{33}\right]^{\mathbf{T}}. \tag{20}$$

Additional special cases are presented in Appendix A.

EXAMPLE 1 - 2-D SHEARED CARTESIAN COORDINATES

An instructive example is a coordinate system formed by a shearing action on a Cartesian mesh (see figure 1). A sheared Cartesian coordinate system is defined by,

$$\begin{bmatrix} x_1 \\ x_2 \\ x_3 \end{bmatrix} = \begin{bmatrix} 1 & 0 & \cos\theta \\ 0 & 1 & 0 \\ 0 & 0 & \sin\theta \end{bmatrix} \begin{bmatrix} \xi_1 \\ \xi_2 \\ \xi_3 \end{bmatrix}, \tag{21}$$

where θ is the shear angle of the coordinate system ($\theta = 90^\circ$ is Cartesian). This system reduces to a more workable set of two equations,

$$\begin{bmatrix} x_1 \\ x_3 \end{bmatrix} = \begin{bmatrix} 1 & \cos\theta \\ 0 & \sin\theta \end{bmatrix} \begin{bmatrix} \xi_1 \\ \xi_3 \end{bmatrix}, \tag{22}$$

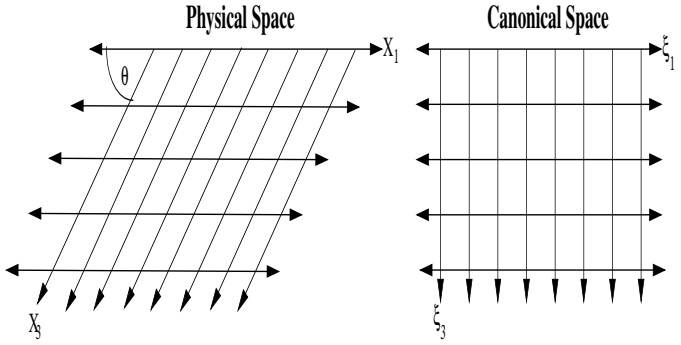

Figure 1: 2-D sheared Cartesian coordinates. Left panel: Physical domain represented by sheared Cartesian coordinates defined by $\{x_1, x_3\}$; Right panel: GRWE domain chosen to be the unit square $\{\xi_1, \xi_2\}$. jeff1-2Dexamp [NR]

that has a metric tensor g_{ij} given by,

$$\left[g_{ij}\right] = \begin{bmatrix} \frac{\partial x_k}{\partial \xi_1}\frac{\partial x_k}{\partial \xi_1} & \frac{\partial x_k}{\partial \xi_1}\frac{\partial x_k}{\partial \xi_3} \\ \frac{\partial x_k}{\partial \xi_1}\frac{\partial x_k}{\partial \xi_3} & \frac{\partial x_k}{\partial \xi_3}\frac{\partial x_k}{\partial \xi_3} \end{bmatrix} = \begin{bmatrix} g_{11} & g_{13} \\ g_{13} & g_{33} \end{bmatrix} = \begin{bmatrix} 1 & \cos\theta \\ \cos\theta & 1 \end{bmatrix}, \tag{23}$$

with a determinant $|\mathbf{g}| = \sin^2\theta$ and an associated metric tensor g^{ij} given by,

$$\left[g^{ij}\right] = \frac{1}{\sin^2\theta}\begin{bmatrix} 1 & -\cos\theta \\ -\cos\theta & 1 \end{bmatrix}. \tag{24}$$

Note that because the tensor in equation 24 is coordinate invariant, equation 10 simplifies to,

$$\Delta \mathcal{U} = g^{ij}\frac{\partial^2 \mathcal{U}}{\partial \xi_i \partial \xi_j} = -\omega^2 s^2 \mathcal{U}, \tag{25}$$

and generates the following dispersion relation,

$$g^{ij} k_{\xi_i} k_{\xi_j} = \omega^2 s^2. \tag{26}$$

Expanding out these terms leads to an expression for wavenumber k_{ξ_3},

$$k_{\xi_3} = -\frac{g^{13}}{g^{33}}k_{\xi_1} \pm \sqrt{\frac{s^2\omega^2}{g^{33}} - \left(\frac{g^{11}}{g^{33}} - \left(\frac{g^{13}}{g^{33}}\right)^2\right)k_{\xi_1}^2}. \tag{27}$$

Substituting the values of the associated metric tensor in equation 24 into equation 27 yields,

$$k_{\xi_3} = \cos\theta\ \mathrm{k}_{\xi_1} \pm \sin\theta\sqrt{\mathrm{s}^2\omega^2 - \mathrm{k}_{\xi_1}^2}. \tag{28}$$

A numerical test using a Cartesian coordinate system sheared at 25° from vertical is shown in figure 2. The background velocity model is 1500 ms^{-1} and the zero-offset data consist of 4 flat plane-waves $t = 0.2, 0.4, 0.6$ and 0.8 s. As expected, the zero-offset migration results image reflectors at depths z=300, 600, 900, and 1200 m. Note that the propagation has created boundary artifacts: those on the left are reflections due to a truncated coordinate system while those on the right are hyperbolic diffractions caused by truncated plane-waves.

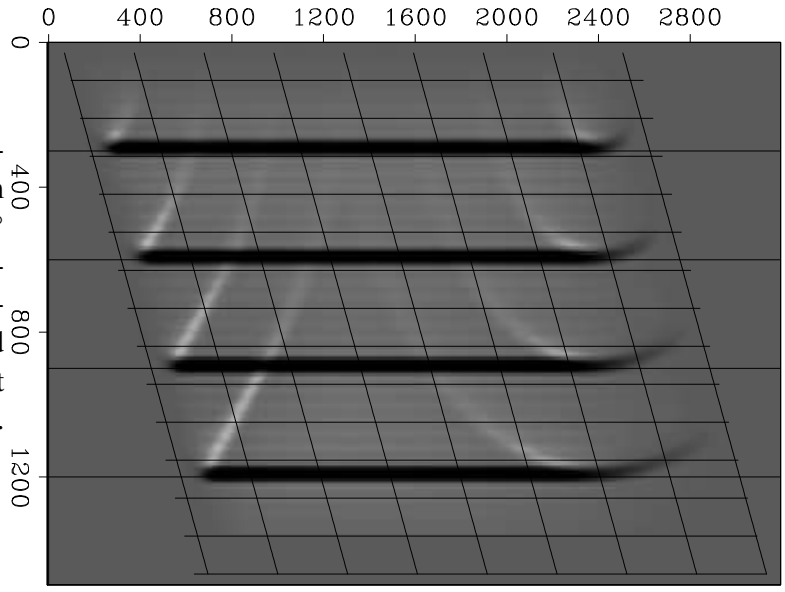

Figure 2: Sheared Cartesian coordinate system test. Coordinate system shear angle and velocity are $\theta = 25°$ and 1500 ms^{-1}, respectively. Zero-offset data consist of 4 flat plane-wave impulses at $t = 0.2, 0.4, 0.6$ and 0.8 s that are correctly imaged at depths $z = 300, 600, 900$, and $1200\,m$. jeff1-Rays0 [ER]

EXAMPLE 2 - POLAR ELLIPSOIDAL

A second instructive example is a stretched polar coordinate system (see figure 3). A polar ellipsoidal coordinate system is specified by,

$$\begin{bmatrix} x_1 \\ x_3 \end{bmatrix} = \begin{bmatrix} a(\xi_3)\xi_1 \cos\xi_3 \\ a(\xi_3)\xi_1 \sin\xi_3 \end{bmatrix}. \tag{29}$$

Parameter $a = a(\xi_3)$ is a smooth function controlling coordinate system ellipticity and has curvature parameters $b = \frac{\partial a}{\partial \xi_3}$ and $c = \frac{\partial^2 a}{\partial \xi_3^2}$. The metric tensor g_{ij} is,

$$\begin{bmatrix} g_{ij} \end{bmatrix} = \begin{bmatrix} a^2 & \xi_1 a\, b \\ \xi_1 a\, b & \xi_1^2(b^2 + a^2) \end{bmatrix}, \tag{30}$$

with determinant $|\mathbf{g}| = a^4\xi_1^2$. The associated metric and weighted associated metric tensors are given by,

$$\begin{bmatrix} g^{ij} \end{bmatrix} = \begin{bmatrix} \frac{b^2+a^2}{a^4} & -\frac{b}{a^3\xi_1} \\ -\frac{b}{a^3\xi_1} & \frac{1}{a^2\xi_1^2} \end{bmatrix} \quad \text{and} \quad \begin{bmatrix} m^{ij} \end{bmatrix} = \begin{bmatrix} \frac{\xi_1(b^2+a^2)}{a^2} & -\frac{b}{a} \\ -\frac{b}{a} & \frac{1}{\xi_1} \end{bmatrix}. \tag{31}$$

Tensors g^{ij} and m^{ij} specify a wavenumber appropriate for extrapolating wavefields on a 2-D non-orthogonal mesh (see equation A-7). However, because the coordinate system is spatially variant, we must also compute the n_i fields: $n_1 = \frac{a^2+2b^2-ac}{a^2}$ and $n_3 = 0$. Inserting these values yields the following extrapolation wavenumber k_{ξ_3},

$$k_{\xi_3} = \frac{\xi_1 b}{a} k_{\xi_1} \pm \sqrt{a^2\xi_1^2 s^2\omega^2 - \xi_1^2 k_{\xi_1}^2 - i k_{\xi_1}\xi_1 \left(\frac{a^2+2b^2-ac}{a^2}\right)}. \tag{32}$$

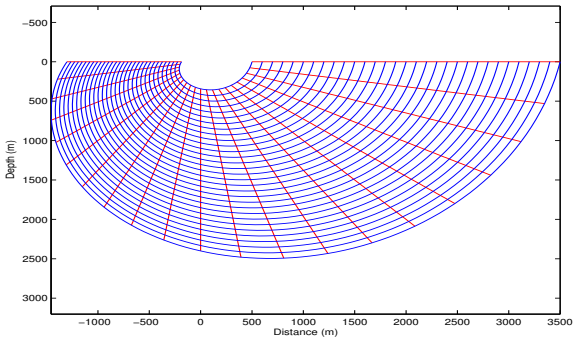

Figure 3: Polar ellipsoidal coordinate system example. jeff1-2Dex2 [NR]

The kinematic version of equation 32 is,

$$k_{\xi_3} = \xi_1 \left[\frac{b}{a} k_{\xi_1} \pm \sqrt{a^2 s^2 \omega^2 - k_{\xi_1}^2} \right], \tag{33}$$

while the orthogonal polar case (i.e. $a = 1$) recovers the following,

$$k_{\xi_3} = \pm \xi_1 \sqrt{s^2 \omega^2 - k_{\xi_1}^2}. \tag{34}$$

Figure 4 shows an ellipsoidal polar coordinate system defined by $a = 1 + 0.2\,\xi_3 - 0.05\,\xi_3^2$. The upper left panel shows a $v(z) = 1500 + 0.2\,z$ velocity function overlain by a coordinate system mesh. The upper right panel presents velocity model as mapped into the GRWE domain. The data used in this test consisted of 4 flat plane-waves. Given this experimental setup, propagating flat plane-waves should not bend in the Cartesian domain because of the $v = v(z)$ velocity model, even though there is velocity variation across each extrapolation step in the GRWE domain. Hence, the impulses have curvature in the GRWE domain (lower right panel). The lower left panel shows the GRWE domain imaging results mapped back to a Cartesian domain. Consistent with theory, the flat plane-waves are imaged as flat reflectors. Note that the edge effects are again caused by coordinate system and plane-wave truncation.

EXAMPLE 3 - GRWE GREEN'S FUNCTION GENERATION

The final test uses GRWE to generate estimates of Green's functions. The test velocity model is a slice of the SEG-EAGE salt model (see figure 5). The contrast between the salt body and sediment velocities cause the wavefield to exhibit complicated propagation including significant wavefield triplication and multipathing. The upper left panel shows the velocity model with an overlain coordinate mesh generated by the differential method discussed in Shragge (2006a). The mesh is a ray-based coordinate system because the first and last extrapolation steps are formed by the 0.04 s and 2.25 s travel-time isochrons from a first-arrival Eikonal equation solution. The velocity model in the GRWE domain is illustrated in the upper right panel.

The lower right panel shows the impulse response test in the GRWE domain. The 7 impulsive waves conform fairly well to the travel-time steps, except where they enter the salt body to

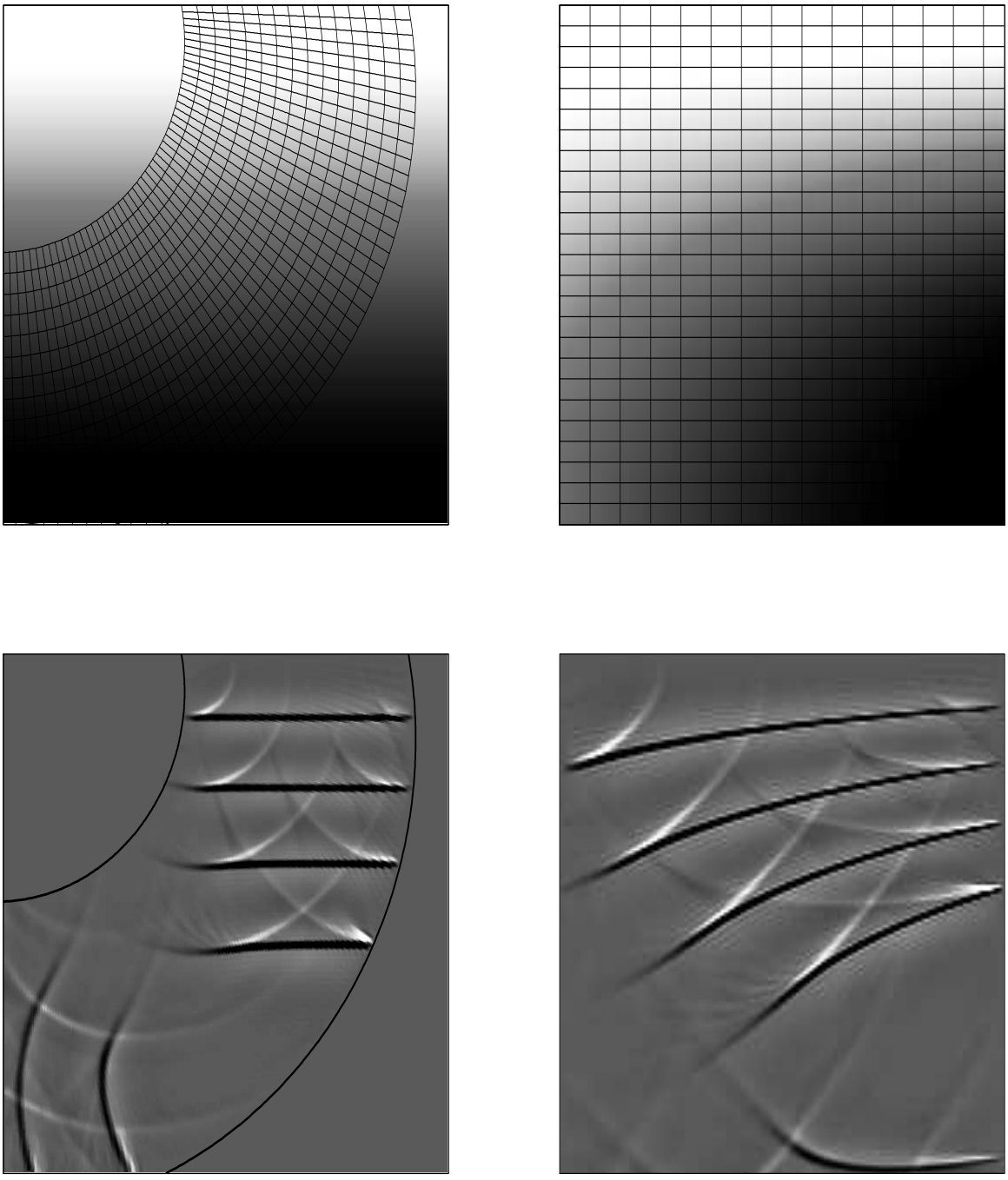

Figure 4: Ellipsoidal polar coordinate system test example. Upper left: $v(z) = 1500 + 0.2\,z$ velocity function overlain by a polar ellipsoidal coordinate system defined by parameter $a = 1 + 0.2\,\xi_3 - 0.05\,\xi_3^2$. Upper right: velocity model in the GRWE domain. Bottom right: Imaged reflectors in GRWE domain. Bottom left: the GRWE domain image mapped to a Cartesian mesh. jeff1-Polar [ER]

the lower left of the image. The migration results mapped back to Cartesian space are shown in the lower left panel. The wavefield to the left of the shot point is fairly complicated and the energy in the salt body and the corresponding upward refracted (and perhaps reflected?) wavefields are strongly present. Figure 6 presents a comparison test between GRWE and Cartesian extrapolation. Beneath and to the right of the shot point the wavefields are fairly similar except for a phase-change. However, they are significantly different to the left because Cartesian-based extrapolation cannot propagate energy laterally with the same accuracy and upward at all. Hence, this energy is absent from the wavefield in the lower panel.

CONCLUDING REMARKS

This paper extends the theory of Riemannian wavefield extrapolation to generalized 3D non-orthogonal coordinate systems. The extrapolation wavenumber decouples from the other wavenumbers allowing us to use an extended split-step Fourier approximate solution. The examples indicate that wavefields can be extrapolated on non-orthogonal coordinate meshes. This generalization allows users to design meshes that have smoother mixed-domain fields that should lead to more accurate and efficient GRWE.

ACKNOWLEDGEMENTS

I acknowledge the contributions of Paul Sava and Sergey Fomel in laying the groundwork for the current theory and thanks to Brad Artman for enlightening discussions.

REFERENCES

Gazdag, J. and P. Sguazzero, 1984, Migration of seismic data by phase-shift plus interpolation: Geophysics, **69**, 124–131.

Guggenheimer, H., 1977, Differential Geometry: Dover Publications, Inc., New York.

Sava, P. and S. Fomel, 2005, Riemannian wavefield extrapolation: Geophysics, **70**, T45–T56.

Shragge, J. and P. Sava, 2004, Incorporating topography into wave-equation imaging through conformal mapping: SEP–**117**, 27–42.

Shragge, J., 2006a, Generalized riemannian wavefield extrapolation: SEP–**124**.

Shragge, J., 2006b, Structured mesh generation using differential methods: SEP–**124**.

Stoffa, P. L., J. T. Fokkema, R. M. de Luna Freire, and W. P. Kessinger, 1990, Split-step Fourier migration: Geophysics, **55**, no. 04, 410–421.

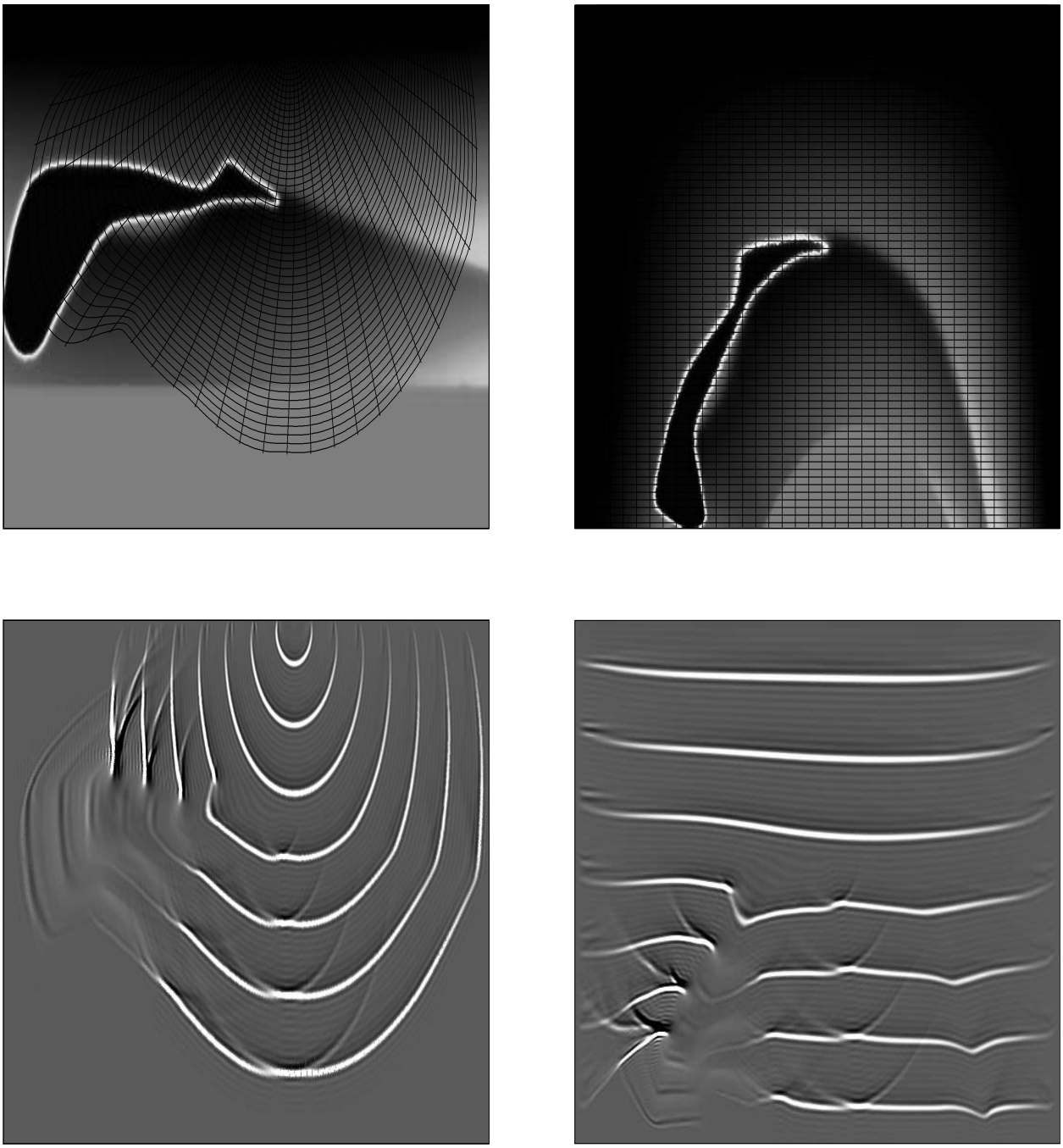

Figure 5: Example of GRWE generated Green's Functions on structured non-orthogonal mesh for a slice through the SEG-EAGE Salt data set velocity model. Top left: Salt model in physical space with an overlain ray-based mesh. Top right: Velocity model in the GRWE domain. Bottom right: Wavefield propagated in ray-coordinates through velocity model shown in the upper right. Bottom left: Wavefield in bottom right interpolated back to Cartesian space. jeff1-SPexamp [ER]

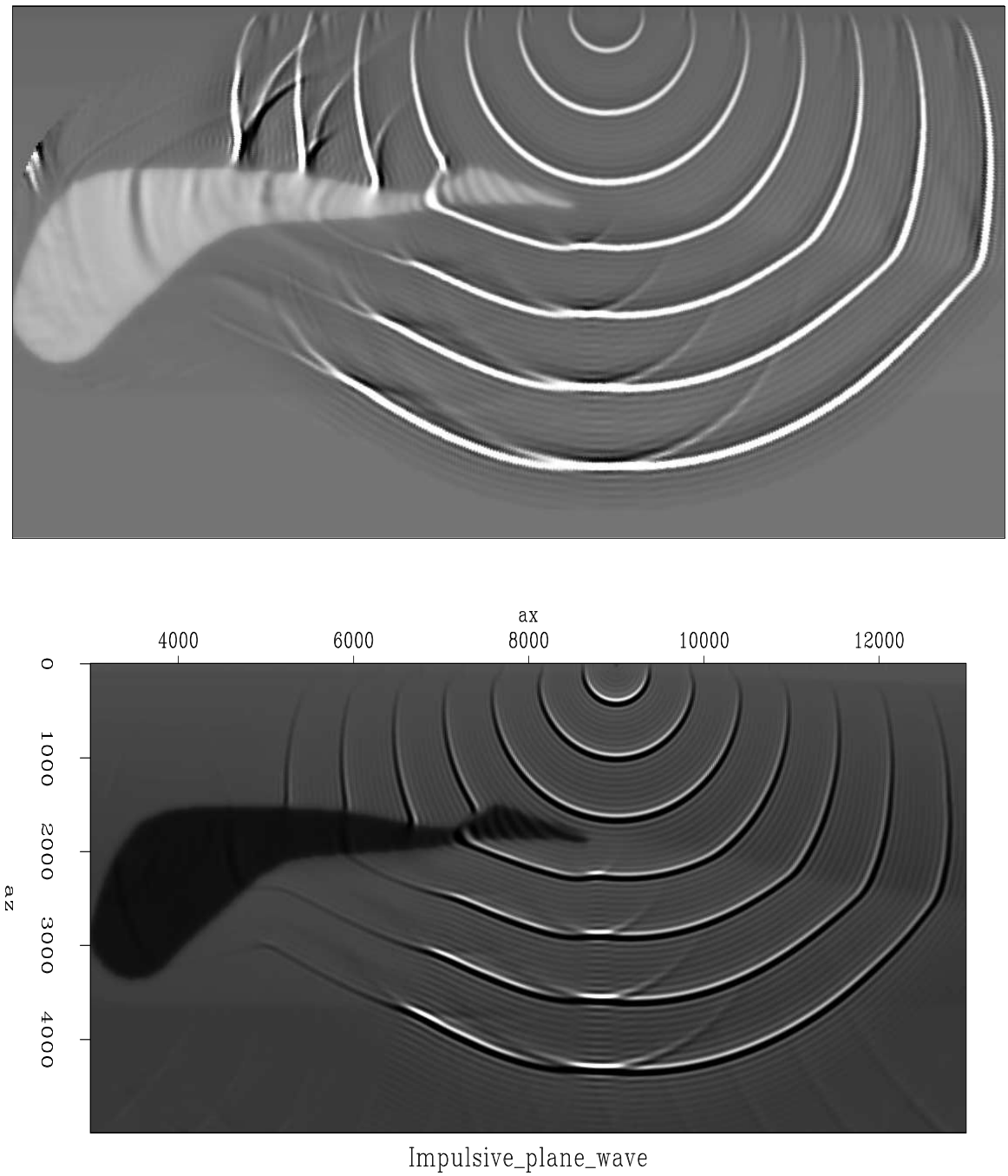

Figure 6: Results of a comparison test between generalized Riemannian wavefield extrapolation (top panel) and Cartesian-based extrapolation (bottom panel). jeff1-SPcompare [ER]

APPENDIX A

The extrapolation wavenumber developed in equation 14 is appropriate for any non-orthogonal Riemannian geometry. However, there are a number of situations where symmetry or partial orthogonality are present. Moreover, one may wish to make a kinematic approximation where all of the imaginary components of the wavenumber are ignored. These situations are discussed in this Appendix.

3D Semi-orthogonal Coordinate Systems - Semi-orthogonal coordinate systems occur where one coordinate is orthogonal to the other two coordinates (Sava and Fomel, 2005). In these cases the m^{13} and m^{23} components of the weighted metric tensor are identically zero, which leads to the following extrapolation wavenumber,

$$k_{\xi_3} = i a_3 \pm \left[a_4^2\omega^2 - a_5^2 k_{\xi_1}^2 - a_6^2 k_{\xi_2}^2 - a_7 k_{\xi_1} k_{\xi_2} + i a_8 k_{\xi_1} + i a_9 k_{\xi_2} - a_{10}^2\right]^{\frac{1}{2}}, \tag{A-1}$$

where,

$$\mathbf{a} = \left[0 \;\; 0 \;\; \frac{n_3}{2m^{33}} \;\; \frac{s}{\sqrt{g^{33}}} \;\; \sqrt{\frac{g^{11}}{g^{33}}} \;\; \sqrt{\frac{g^{22}}{g^{33}}} \;\; \frac{2g^{12}}{g^{33}} \;\; \frac{n_1}{m^{33}} \;\; \frac{n_2}{m^{33}} \;\; \frac{n_3}{m^{33}}\right]^{\mathbf{T}}. \tag{A-2}$$

which are the coefficients recovered by Sava and Fomel (2005).

3-D Kinematic Coordinate Systems - Wave-equation migration amplitudes are generally inexact in laterally variant media - even in a Cartesian based system. Hence, one beneficial approximation that reduces computational cost is to consider only the kinematic terms in equation 14. This approximate generates the following extrapolation wavenumber,

$$k_{\xi_3} = a_1 k_{\xi_1} + a_2 k_{\xi_2} \pm \left[a_4^2\omega^2 - a_5^2 k_{\xi_1}^2 - a_6^2 k_{\xi_2}^2 - a_7 k_{\xi_1} k_{\xi_2} - a_{10}^2\right]^{\frac{1}{2}}, \tag{A-3}$$

where,

$$\mathbf{a} = \left[-\frac{g^{13}}{g^{33}} \;\; -\frac{g^{23}}{g^{33}} \;\; 0 \;\; \frac{s}{\sqrt{g^{33}}} \;\; \sqrt{\frac{g^{11}}{g^{33}} - \left(\frac{g^{13}}{g^{33}}\right)^2} \;\; \sqrt{\frac{g^{22}}{g^{33}} - \left(\frac{g^{23}}{g^{33}}\right)^2} \;\; \frac{2g^{12}}{g^{33}} - \frac{2g^{13}g^{23}}{\left(g^{33}\right)^2} \;\; 0 \;\; 0 \;\; \frac{n_3}{m^{33}}\right]^{\mathbf{T}}. \tag{A-4}$$

3-D Kinematic Semi-orthogonal coordinate systems - Combining the two above restrictions yields the following extrapolation wavenumber,

$$k_{\xi_3} = \pm\left[a_4^2\omega^2 - a_5^2 k_{\xi_1}^2 - a_6^2 k_{\xi_2}^2 - a_7 k_{\xi_1} k_{\xi_2} - a_{10}^2\right]^{\frac{1}{2}}, \tag{A-5}$$

where,

$$\mathbf{a} = \left[0 \;\; 0 \;\; 0 \;\; \frac{s}{\sqrt{g^{33}}} \;\; \sqrt{\frac{g^{11}}{g^{33}} - \left(\frac{g^{13}}{g^{33}}\right)^2} \;\; \sqrt{\frac{g^{22}}{g^{33}} - \left(\frac{g^{23}}{g^{33}}\right)^2} \;\; \frac{2g^{12}}{g^{33}} - \frac{2g^{13}g^{23}}{\left(g^{33}\right)^2} \;\; 0 \;\; 0 \;\; \frac{n_3}{m^{33}}\right]^{\mathbf{T}}. \tag{A-6}$$

Note that the expression $\Phi = 1$, and that components of the metric tensor are significantly simplified.

2-D Non-orthogonal coordinate systems - Two-dimensional situations are handled by identifying $\xi_2 = 0$. Hence, all derivatives in the associated metric tensor g^{ij} with respect coordinate ξ_2 are identically zero. Hence, a 2-D non-orthogonal coordinate system can be represented by

$$k_{\xi_3} = a_1 k_{\xi_1} + i a_3 \pm \left[a_4^2\omega^2 - a_5^2 k_{\xi_1}^2 + a_8 i k_{\xi_1} - a_{10}^2\right]^{\frac{1}{2}}, \tag{A-7}$$

where,

$$\mathbf{a} = \left[-\frac{g^{13}}{g^{33}} \;\; 0 \;\; \frac{n_3}{2m^{33}} \;\; \frac{s}{\sqrt{g^{33}}} \;\; \sqrt{\frac{g^{11}}{g^{33}} - \left(\frac{g^{13}}{g^{33}}\right)^2} \;\; 0 \;\; 0 \;\; \frac{n_1}{m^{33}} \;\; 0 \;\; \frac{n_3}{m^{33}}\right]^{\mathbf{T}}. \tag{A-8}$$

2-D Non-orthogonal Kinematic Coordinate Systems - Two-dimensional kinematic situations are handled through identity $\xi_2 = 0$. Again, all derivatives in the associated metric tensor g^{ij} with respect coordinate ξ_2 are identically zero, and the 2-D non-orthogonal kinematic extrapolation wavenumber is

$$k_{\xi_3} = a_1 k_{\xi_1} \pm \left[a_4^2\omega^2 - a_5^2 k_{\xi_1}^2 - a_{10}^2\right]^{\frac{1}{2}}, \tag{A-9}$$

where,

$$\mathbf{a} = \left[-\frac{g^{13}}{g^{33}} \;\; 0 \;\; 0 \;\; \frac{s}{\sqrt{g^{33}}} \;\; \sqrt{\frac{g^{11}}{g^{33}} - \left(\frac{g^{13}}{g^{33}}\right)^2} \;\; 0 \;\; 0 \;\; 0 \;\; 0 \;\; \frac{n_3}{m^{33}}\right]^{\mathbf{T}}. \tag{A-10}$$

2-D Orthogonal Coordinate Systems - Two-dimensional situations are handled with $\xi_2 = g_{13} = 0$. Accordingly, all derivatives in the associated metric tensor g^{ij} with respect coordinate ξ_2 are identically zero, and the 2-D non-orthogonal coordinate system is represented by

$$k_{\xi_3} = i a_3 \pm \left[a_4^2\omega^2 - a_5^2 k_{\xi_1}^2 + i a_8 k_{\xi_1} - a_{10}^2\right]^{\frac{1}{2}}, \tag{A-11}$$

where,

$$\mathbf{a} = \left[0 \;\; 0 \;\; \frac{n_3}{2m^{33}} \;\; \frac{s}{\sqrt{g^{33}}} \;\; \sqrt{\frac{g^{11}}{g^{33}} - \left(\frac{g^{13}}{g^{33}}\right)^2} \;\; 0 \;\; 0 \;\; \frac{n_1}{m^{33}} \;\; 0 \;\; \frac{n_3}{m^{33}}\right]^{\mathbf{T}}. \tag{A-12}$$

2-D Orthogonal Kinematic Coordinate Systems - The above two approximations can be combined to yield the following extrapolation wavenumber for 2-D orthogonal kinematic coordinate systems,

$$k_{\xi_3} = \pm \left[a_4^2\omega^2 - a_5^2 k_{\xi_1}^2 - a_{10}^2\right]^{\frac{1}{2}}, \tag{A-13}$$

where,

$$\mathbf{a} = \left[0 \;\; 0 \;\; 0 \;\; \frac{s}{\sqrt{g^{33}}} \;\; \sqrt{\frac{g^{11}}{g^{33}} - \left(\frac{g^{13}}{g^{33}}\right)^2} \;\; 0 \;\; 0 \;\; 0 \;\; 0 \;\; \frac{n_3}{m^{33}}\right]^{\mathbf{T}}. \tag{A-14}$$